Polymer 51 (2010) 4195–4199

Contents lists available at ScienceDirect

Polymer

journal homepage: www.elsevier.com/locate/polymer

Determination of lamella thickness distributions in isotactic polypropylene by X-ray line profile analysis

Florian Spieckermann [a,*], Harald Wilhelm [a,b], Michael Kerber [a], Erhard Schafler [a], Gerald Polt [a], Sigrid Bernstorff [c], Frédéric Addiego [d], Michael Zehetbauer [a]

[a] Research Group Physics of Nanostructured Materials, Faculty of Physics, University of Vienna, Boltzmanngasse 5, 1090 Wien, Austria
[b] Laboratory of Polymer Engineering LKT-TGM, Wexstrasse 19-23, 1200 Wien, Austria
[c] Sincrotrone Trieste, Strada Statale 14 km 163.5 in AREA Science Park, 34149 Basovizza, Trieste, Italy
[d] CRP Henri Tudor, Advanced Materials and Structures Department, 66 rue de Luxembourg, L-4221 Esch sur Alzette, Luxembourg

ARTICLE INFO

Article history:
Received 18 February 2010
Received in revised form
26 June 2010
Accepted 6 July 2010
Available online 14 July 2010

Keywords:
Polypropylene
Lamella thickness
Bragg profile analysis

ABSTRACT

X-ray line profile analysis was used to determine the size distribution of the crystalline lamellae in isotactic polypropylene (iPP) assuming a log-normal size distribution. A comparison with the size distribution as determined by differential scanning calorimetry (DSC) yields an excellent agreement of both methods. It is noted that the agreement depends strongly on whether linear lattice defects, particularly dislocations are taken into account in the X-ray analysis. This is especially true for deformed iPP with a high number of deformation induced dislocations. It was also found that for a multimodal distribution of lamella thickness in the DSC experiment as induced by the introduction of titanium dioxide nanoparticles as filler material the lamella thickness distribution from X-ray profile analysis is still in good agreement with DSC although the model used was only monomodal.

© 2010 Elsevier Ltd. All rights reserved.

1. Introduction

The deformation mechanisms and thus the mechanical properties of semicrystalline polymers depend strongly on the microstructure. Particularly the thickness of the crystalline lamellae seems to be a crucial parameter with respect to the mechanical strength [1].

For the determination of the lamella thickness in semicrystalline polymers several experimental methods exist, including differential scanning calorimetry (DSC), small angle X-ray scattering (SAXS), electron microscopy and optical methods. Attempts were also made to determine the crystallite size by evaluation of wide angle X-ray scattering (WAXS) profiles using the width of the Bragg-peaks through a separation of size broadening and broadening caused by statistical lattice defects, the latter commonly described by models of paracrystallinity [2–4].

In the present paper the crystallite size distribution in α-nucleated isotactic polypropylene is determined using a Bragg-peak-profile analysis method that has so far not found extensive application in polymeric materials. In contrast to the earlier investigations the present work uses multi reflection X-ray line profile analysis (MXPA), which takes into account several Bragg reflections (optimally also the upper harmonics of a reflection). From investigations in metals and ceramics [5–7] it is known that the procedure allows to determine the size distribution and the shape of the crystallites with a high reliability from a single WAXS pattern. To check the validity of the method in the semicrystalline polymer iPP the resultant size distributions are compared to distributions obtained from DSC.

2. Theory

2.1. Multi reflection X-ray line profile analysis (MXPA)

In the kinematic theory of X-ray diffraction the physical profile of a Bragg reflection is given by the convolution of the intensity profiles caused by finite size and by lattice distortions. The logarithm of the Fourier transform yields the well known Warren–Averbach formula [8]

$$\ln A(L) = \ln A^S(L) + \ln A^D(L) \quad (1)$$

where $A(L)$ are the Fourier coefficients of the Bragg profile (L is the Fourier length), $A^S(L)$ and $A^D(L)$ are the coefficients related to the the size and the strain broadening respectively. The strain broadening is modeled by assuming that it is caused by the mean square strain $\langle \epsilon^2 \rangle$ leading to a Fourier coefficient $A^D(L)$ of the form

* Corresponding author. Tel.: +43 1 4277 51299; fax: +43 1 4277 51440.
E-mail address: florian.spieckermann@univie.ac.at (F. Spieckermann).

0032-3861/$ – see front matter © 2010 Elsevier Ltd. All rights reserved.
doi:10.1016/j.polymer.2010.07.009

$$A^D(L) = \exp\left(-2\pi^2 L^2 k^2 \left\langle \epsilon^2 \right\rangle\right) \quad (2)$$

with k the diffraction vector.

For the evaluation of crystalline defects the characteristic anisotropy of $\langle \epsilon^2 \rangle$ can be related to the defects in question thus allowing for a separation of the broadening related to the size and to crystalline defects of linear (dislocations) and planar nature (twins, stacking faults) [9,10]. In the present case only dislocations were considered.

As nucleation controlled crystallisation processes often lead to a log-normal size distribution [11], the peak broadening caused by the finite size is taken into account by such a distribution. The corresponding density distribution function of the size λ has the form

$$f(\lambda) = \frac{1}{\lambda\sigma\sqrt{2\pi}} \exp - \frac{(\ln \lambda - \ln m)^2}{2\sigma^2} \quad (3)$$

with the parameters m and σ where $\mu = \ln m$ is the median and σ is the variance of the distribution.

For the evaluation of the X-ray line broadening the program *CMWP-fit* (Convolutional Multiple Whole Profile fitting), developed by Ribarik et al. [12,13], was used as it provides a very sophisticated and flexible evaluation procedure. In the software, the size broadening is taken into account by assuming a log-normal distribution (Eq. (3)) with the fitting parameters $b = \ln m$ and $c = \sqrt{2}\sigma$.

The shape of the crystallites is modeled as rotation ellipsoids with an ellipticity parameter ϵ also possible to be fitted by *CMWP-fit*. The model parameters related to the dislocation broadening are a_1, …, a_5 (for the average dislocation contrast factor $\overline{C}$ of an orthorhombic[1] lattice), d (related to the dislocation density $\rho = 2/(\pi B^2 d^2)$, $B = 0.22$ nm [15] being the burgers vector) and e (related to the dislocation cut-off radius $R_e^* = \exp(-1/4)/(2e)$). Furthermore the intensity and position of each Bragg-peak can be fit-parameters in *CMWP-fit*. All fit parameters in *CMWP-fit* can be fixed to a certain value. This is essential to restrict the number of parameters to be determined from fitting to the unknown quantities. The peak positions and intensities as well as the contrast parameters a_1, …, a_5 are typical examples of parameters that can be determined independently, thus allowing to hold them fixed in the evaluation with *CMWP-fit*.

The effect of defect induced broadening can be directly inspected using the Williamson and Hall method [16] and its modified version [9,17]. Plotting the full width at half maximum k_{FWHM} of the peaks as a function of their diffraction vector k allows for a first simple separation of the effects of size and strain broadening. Any deviation of the data from a monotonous behaviour is an indication of anisotropic strains. Assuming that the anisotropic strains are caused by dislocations, the modified Williamson–Hall plot accounts for the defect-specific broadening using the average contrast factor for dislocations $\overline{C}$. Plotting the peak width as a function of $k\sqrt{\overline{C}}$ should result in a monotonic behaviour if the anisotropy is correctly described by the model used for the distortions [9,14,17].

2.2. Lamella thickness distributions from DSC

DSC experiments can be used as a tool for the determination of crystal thickness distributions in semicrystalline homopolymers [18–20]. This procedure has the advantage to be a fast method with simple sample preparation resulting in an integral information over the whole sample volume. Yet several aspects have to be considered in order to obtain correct size distributions most notably the effects of the melting kinetics of the investigated polymer as well as effects due to the calorimeter used. The determination of size distributions from DSC builds on the fact that the melting temperature T_m is related to the thickness λ of the plate-like crystallites by the Gibbs–Thomson equation

$$T_m = T_m^0 \left(1 - \frac{2\sigma_e}{\Delta h_c \lambda}\right). \quad (4)$$

For α-iPP the free fold surface energy is assumed as $\sigma_e = 0.07$ J/m^2, the equilibrium melting point of the 100% crystalline material as $T_m^0 = 187.5$ °C (= 460.65 K) [21,22]. The heat of fusion per unit volume Δh_c is calculated from the heat of fusion of an ideally crystalline sample ($\Delta H^0 = 207$ J/g) on the basis of the density of perfectly crystalline α-iPP $\rho_c = 936$ kg/m^3 and T_m is the melting temperature as derived from the DSC experiments [21,22].

In order to derive the lamella thickness distribution from the DSC experiment (measuring $P(T)$, the power absorbed at temperature T), Alberola et al. [23] and later Crist and Mirrabella [20] showed that a derivative formulation has to be considered. This is necessary because the DSC signal $P(T)$ is proportional to the melting distribution and cannot be used directly as a size distribution function as it was done by some authors. The resulting size distribution function for a constant heating rate $\beta = dT/dt$ was found as

$$g(\lambda) = \frac{P(T)}{\alpha_m \Delta H^0 M(\mathrm{d}T/\mathrm{d}t)} \frac{\mathrm{d}T}{\mathrm{d}\lambda} \quad (5)$$

where α_m is the mass fraction crystallinity and M the sample mass. Setting $T_m = T$, substituting Eq. (4) in Eq. (5) and assuming Δh_c to be temperature independent allow the size distribution function to be written as:

$$g(\lambda) = KP(T)\left(T_m^0 - T\right)^2. \quad (6)$$

The normalisation constant K can be considered as temperature independent and is therefore determined by numerical integration of $P(T)(T_m^0 - T)^2$ [20].

3. Experimental

Isotactic polypropylene BE50 by Borealis company, which is delivered with an α-nucleation agent securing nucleation of a homogeneous spherulitic structure, was used. Bars with the dimensions 10 × 10 × 200 mm^3 were cut from an extruded plate. A heat treatment consisting of melting and subsequently recrystallising near the crystallisation temperature $T_c = 165$ °C for 2 h ensured low preferential orientations and a uniform spherulithic size distribution. Cylindrical samples (diameter: 6 mm, height: 10 mm) were machined for X-ray experiments. Platelets with 1 mm thickness were cut with a diamond saw, from which discs of about 20 mg where punched out for differential scanning calorimetry (DSC). The experiments were carried out on a Netzsch DSC 204 calorimeter under argon atmosphere to avoid effects by oxidation or condensation. In order to minimise effects by lamellar thickening, a heating rate of 10 K/min was chosen. The shift of T_m related to the rate sensitivity of the melting kinetics was accounted for by a correction factor determined by linear approximation of the rate dependence of the melting temperature $T_m(\beta)$ (Fig. 1).

WAXS measurements were performed in transmission setup at the SAXS-Beamline 5.2L of the synchrotron ELETTRA (Trieste, Italy). After recording the profile at the undeformed state the sample was deformed up to a true strain of $\epsilon_t = 0.5$ using a miniature compression machine allowing for in situ deformations; several profiles were recorded over the whole deformation range.

[1] It is reasonable to assume an orthorhombic lattice for the contrast calculation as the effect of the monoclinic angle is negligible in first approximation [14].

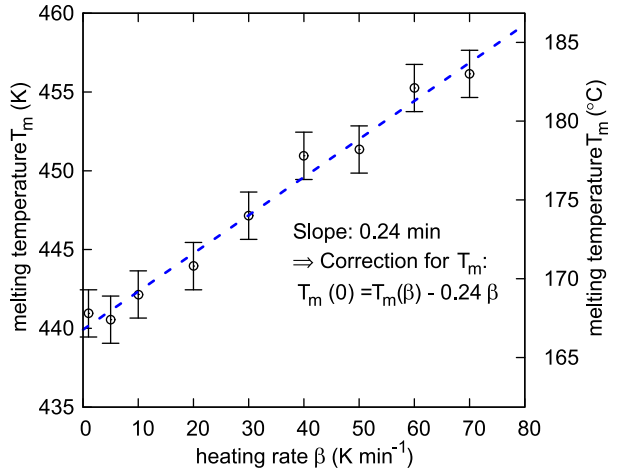

Fig. 1. Offset of the melting temperature T_m as determined by DSC (○) as a function of the heating rate. The slope of the fit (dashed line) amounting to 0.24 min is used to determine $T_m(0)$.

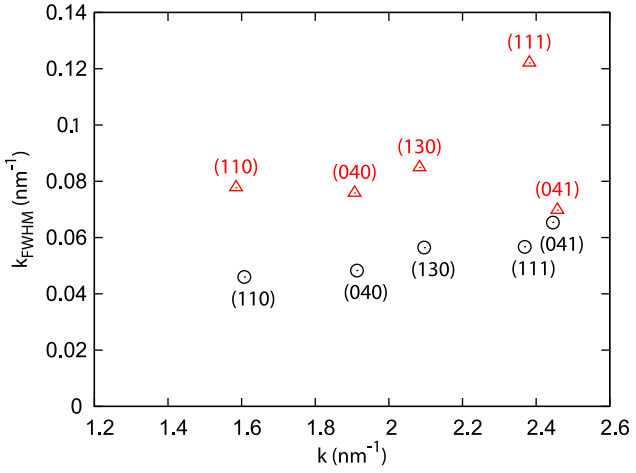

Fig. 3. Williamson–Hall plots of α-iPP before deformation (○), and after deformation up to $\epsilon_t = 0.5$ (△).

Collecting the data under load makes it possible to minimise relaxation effects of the deformed sample.

The photon energy used was 8 keV, which corresponds to a wave length of CuK_α radiation of 0.154 nm. The incident beam had a spot size of 100 μm × 400 μm on the sample and the photon flux amounted to 5×10^{11} photons mm^{-2} s^{-1}. The WAXS spectra were recorded with a linear position-sensitive detector (1024 channels, type PSD 50 of Braun, Munich, Germany) positioned at a distance of 370 mm from the specimen. To ensure sufficient statistics for a reliable evaluation of the Bragg profiles at least 10^4 counts were collected in the maxima of the diffraction peaks.

For comparison further experiments were carried out on samples of the same polypropylene type but filled with a small amount of titanium dioxide (TiO_2) nanoparticles. To this end, 5 wt.% of TiO_2 (Degussa Aeroxide P25, particle size range 20–80 nm) were carefully distributed and dispersed in the iPP matrix by extrusion.

4. Results and discussion

The recorded diffraction patterns were subjected to a pre-evaluation (using *GNU octave* and *fityk* software). In order to properly determine the background mainly arising from the scattering of the amorphous phase a 5th order polynomial is used. A small amount of γ-crystallised iPP resulted in diffraction peaks at known positions. To determine peak positions and intensities of all known phases, the peaks were, in a first step, approximated using Pearson VII functions also giving reasonable widths for each peak. The number of fit parameters was reduced using known ratios of peak positions where possible, greatly improving the reliability. The excellent result of this separation procedure is shown in Fig. 2. For the CMWP procedure, the background and the additional phase were then subtracted in order to obtain exclusively the diffraction profile of the α phase. Furthermore the peak widths fitted in the pre-evaluation were used to determine appropriate parameters for the average contrast factor $\overline{C}$ by Williamson–Hall (W–H) analysis, to be used later on in the *CMWP-fit*. A detailed description of this procedure is given by Wilhelm et al. [14] and Spieckermann et al. [24]. The Willamson–Hall plots of undeformed and deformed α-iPP (Fig. 3) show that the deformation increases the anisotropy of the broadening as indicated by the scattering of the peak width of the deformed sample. The modified Williamson–Hall plot (Fig. 4) shows that by determination of the dislocation contrast factor $\overline{C}$

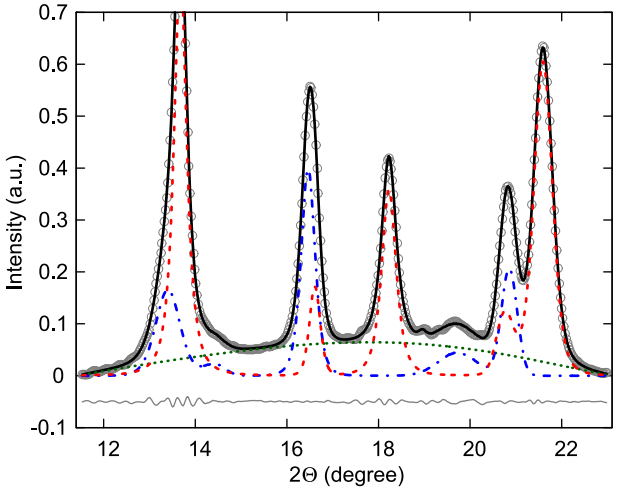

Fig. 2. WAXS pattern of undeformed iPP, measured data (○), fit (full line), α-phase (dashed line), γ-phase (dash-dotted line), amorphous phase (dotted line), residuals (gray line).

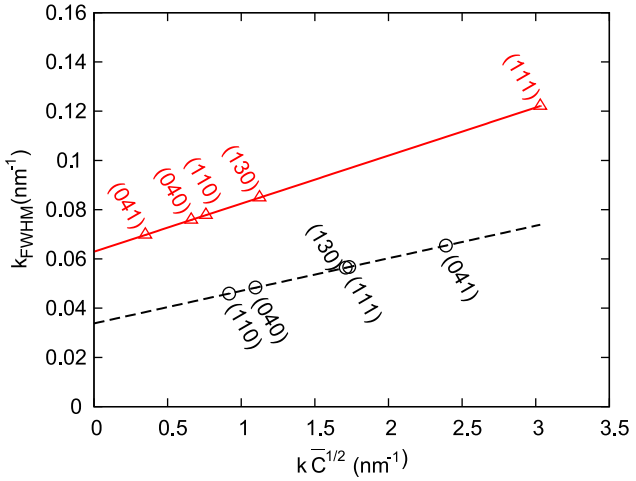

Fig. 4. Modified Williamson–Hall plots of α-iPP before deformation (○), and after deformation up to $\epsilon_t = 0.5$ (△).

Table 1
CMWP-fit Parameters for undeformed α-iPP and related physical quantities.

Param.	Value	Physical quantity	Value
ϵ	0.90	Size ellipticity ϵ	0.90
b	2.79	Size median μ	16.10 nm
c	0.33	Size variance σ	0.24
$a_1 \ldots a_5$	Fixed	Average contrast factor $\overline{C}$	From W–H
d	61.5	Dislocation density ρ	7.6×10^{14} m^{-2}
e	0.04	Dislocation cut-off radius R_e^*	9.6 nm

a linearisation as a function of $k\sqrt{\overline{C}}$ is possible. This is already a strong sign for the presence of dislocations as it was reported by Wilhelm et al. [14]. The slope of the fitted lines is proportional to the square root of the dislocation density [9] and it clearly increases with deformation.

The adapted profiles were consequently evaluated with *CMWP-fit*. The resultant fit parameters and their physical correspondence are given in Table 1 for the undeformed sample and in Table 2 for the sample deformed up to a true strain of $\epsilon_t = 0.5$.

While the diffraction experiments yield the size of the coherently scattering domains (CSD, i.e. the smallest undistorted crystals) the DSC experiments should, according to the theory of Hoffmann and Miller [25], yield the stem length (i.e. the distance of two adjacent fold surfaces along the molecular chain). Hence, both methods provide quantities measured along the crystallographic axes and it is reasonable to attempt a comparison.

The size distribution as determined via DSC is very close to a log-normal distribution, which is common for size distributions resulting from nucleation controlled processes of nanocrystals [5–7]. It is therefore reasonable to approximate the distribution by fitting the corresponding distribution function. When comparing the DSC experiments to the results from the MXPA experiments one finds that both log-normal distributions coincide very well for the melt crystallised α-polypropylene (Fig. 5(a)) as well as for the deformed state (Fig. 5(b)). The dislocation density, also determined via MXPA is increased considerably by the plastic deformation as it can be seen when comparing the results presented in Tables 1 and 2. A reasonable dislocation cut-off radius in the order of the lamella thickness is found and the ϵ-parameter indicates only a slight deviation from the spherical shape.

To study the influence of the crystalline defects on the evaluated size distribution, it was assumed that the crystal is virtually dislocation free for the deformed as well as for the undeformed state. This assumption was modeled in the *CMWP-fit* by fixing the parameter d at a value of 10^5 corresponding to a dislocation density of only $\sim 10^9$ m^{-2}. The resultant size distributions for the deformed and the undeformed case are depicted in Fig. 5 as dotted curves. For the undeformed sample fixing the dislocation density has only marginal effect on the size distribution evaluated via MXPA, attributed to the relatively low dislocation density. This is in contrast to the deformed case where a strong difference to the DSC curve is seen when assuming no dislocations present in the material while including the dislocations in the *CMWP-fit* gives good agreement between DSC and X-ray results.

Table 2
CMWP-fit Parameters for α-iPP deformed up to $\epsilon_t = 0.5$ and related physical quantities.

Param.	Value	Physical quantity	Value
ϵ	1	Size ellipticity ϵ	1
b	2.66	Size median μ	14.30 nm
c	0.25	Size variance σ	0.17
$a_1 \ldots a_5$	Fixed	Average contrast factor $\overline{C}$	From W–H
d	10.55	Dislocation density ρ	1.2×10^{17} m^{-2}
e	0.04	Dislocation cut-off radius R_e^*	8.7 nm

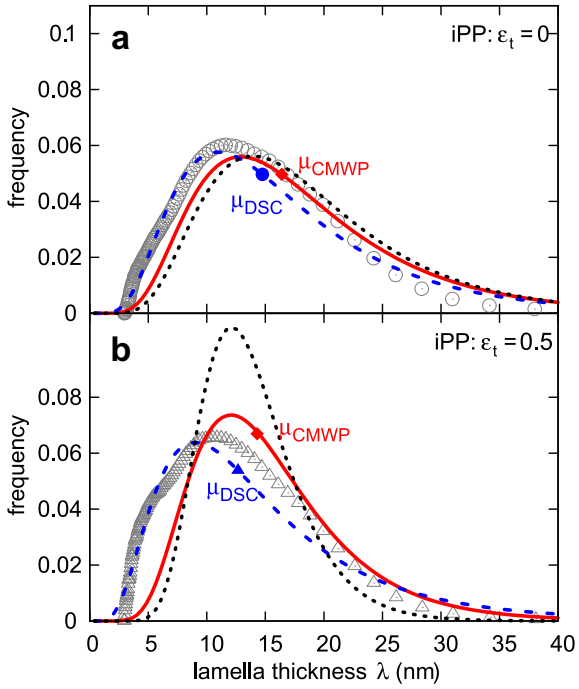

Fig. 5. Lamella thickness distribution determined for (a) undeformed iPP and (b) iPP deformed up to $\epsilon_t = 0.5$ by DSC (undeformed: ○, deformed: △) and MXPA (full line). The dashed lines represent the corresponding log-normal fit of the respective DSC distribution. The respective results of MXPA with very low assumed dislocation densities are plotted as dotted lines.

For the correct determination of the lamellar sizes it is therefore crucial to consider the influence of crystalline defects, especially when their number is high as in case of the deformed sample. Apart from the fact that the quality of the model fit is better when assuming the presence of dislocations these observations are a strong indication that a considerable part of the broadening is caused by linear defects i.e. dislocations. On the other hand the results also show that the broadening in the undeformed state is highly governed by the crystallite size.

Repeating the procedure for the samples filled with 5 wt.% TiO_2 shows that a slight deviation from the monomodal log-normal

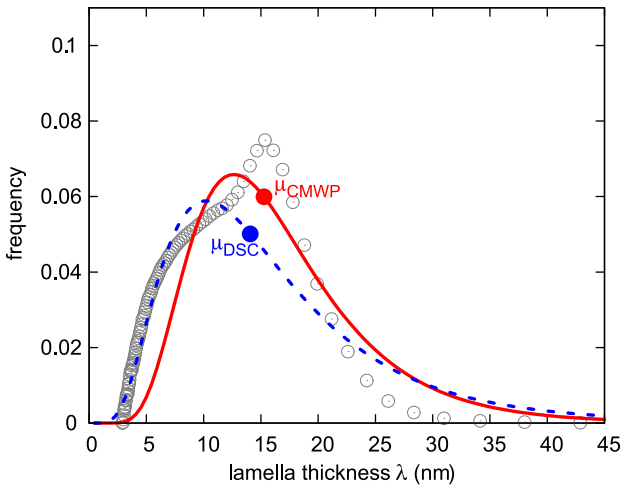

Fig. 6. Lamella thickness distribution determined for iPP-TiO_2 by DSC (○) and MXPA (full line). The dashed line represents the corresponding log-normal fit of the DSC distribution.

Table 3
CMWP-fit Parameters for α-iPP filled with 5 wt.% TiO_2 nanoparticles and related physical quantities.

Param.	Value	Physical quantity	Value
$\in$	0.98	Size ellipticity $\in$	0.98
b	2.73	Size median μ	15.28 nm
c	0.27	Size variance σ	0.19
$a_1 \ldots a_5$	Fixed	Average contrast factor $\overline{C}$	From W–H
d	12.9	Dislocation density ρ	$8.2 \cdot 10^{16}$ m^{-2}
e	0.03	Dislocation cut-off radius R_e^*	12.9 nm

distribution to a bimodal distribution is seen via DSC. Possibly a fraction of the introduced particles hinders crystallisation locally leading to regions that are only poorly crystallised and other regions where crystallisation is not hindered. Such a behaviour could result in the observed bimodal size distribution. Still as a first approximation and in order to compare with the CMWP results, a log-normal distribution is fitted to the DSC size distribution. A reasonable agreement is found and even the medians of the (monomodal) size distributions determined by DSC and MXPA are in fairly good agreement (Fig. 6). The relatively high dislocation density (Table 3) also suggests that the filler interferes in the crystallisation thus also inducing a lower degree of crystalline order.

5. Conclusions

MXPA proved to be effective to determine the size distribution of the crystalline lamellae in α-crystallised polypropylene. The presence of crystalline defects has to be taken into account in order to achieve correct crystallite size distributions. In deformed samples the dislocation density turns out to be markedly higher than in the undeformed state and a correct determination of the size distribution from MXPA is only possible if these dislocations are considered. This supports findings from earlier experiments assuming the presence of dislocations in bulk polypropylene.

The good agreement between X-ray and DSC results opens the possibility to use DSC to determine reasonable starting parameters for MXPA. By direct numerical computation of $A^S(L)$ from $g(\lambda)$ one could even account completely for the size broadening in future X-ray investigations of semicrystalline polymers.

MXPA should also be applicable to other crystallisable polymers, provided that a sufficient number of reflections is detectable. This is necessary to make use of the ability of the method to fully characterise defect induced strains, and thus allow for the correct quantification of the size related part of the line broadening. Indeed first investigations in poly-3(hydroxbuthyrate) [24] also gave reasonable results.

It was also shown that a pitfall in the application of MXPA as a tool for the determination of the crystallite size in semicrystalline polymers lies in the danger to use the wrong model distribution (log-normal, gamma,…) or have a multimodal distribution. This will especially be crucial when dealing with copolymers where monomodal distributions are rare.

Acknowledgements

Funding by the University of Vienna within the PhD Program ‘Experimental Materials Science – Nanostructured Materials’ and the Focus Project ‘Bulk Nanostructured Materials’ is gratefully acknowledged. Dr. Daria Setman and Dr. Thomas Kratochvilla are thanked for advice concerning the DSC experiments and their evaluation.

References

[1] Kazmierczak T, Galeski A, Argon AS. Polymer 2005;46(21):8926–36.
[2] Buchanan DR, Miller RL. J Appl Phys 1966;37(11):4003–12.
[3] Hosemann R, Wilke R, Baltá-Calleja FJ. Acta Crystallogr 1966;21(1):118–23.
[4] Hosemann R, Lange A, Hentschel MP. Acta Crystallogr Sect A 1985;41(5):434–40.
[5] Scardi P, Leoni M. Acta Crystallogr Sect A 2002;58(2):190–200.
[6] Leoni M, Scardi P. J Appl Crystallogr 2004;37(4):629–34.
[7] Ungár T, Gubicza J, Ribárik G, Borbély A. J Appl Crystallogr 2001;34(3):298–310.
[8] Warren BE, Averbach BL. J Appl Phys 1950;21(6):595–9.
[9] Ungár T, Borbély A. Appl Phys Lett 1996;69(21):3173–5.
[10] Ungár T, Tichy G. Phys Status Solidi A 1999;171(2):425–34.
[11] Hinds WC. Aerosol technology: properties, behavior and measurement of airbone particles. New York: Wiley Interscience; 1982.
[12] Ribárik G, Ungár T, Gubicza J. J Appl Crystallogr 2001;34(5):669–76.
[13] Ribárik G, Gubicza J, Ungár T. Mater Sci Eng A 2004;387-389:343–7.
[14] Wilhelm H, Paris A, Schafler E, Bernstorff S, Bonarski J, Ungár T, et al. Mater Sci Eng A 2004;387–389:1018–22.
[15] Séguéla R. J Polym Sci Part B Polym Phys 2002;40:593–601.
[16] Williamson GK, Hall WH. Acta Metall 1953;1(1):22–31.
[17] Kerber M, Schafler E, Zehetbauer M. Rev Adv Mater Sci 2005;10:427–33.
[18] Yamada K, Hikosaka M, Toda A, Yamazaki S, Tagashira K. Macromolecules 2003;36(13):4790–801.
[19] Yamada K, Hikosaka M, Toda A, Yamazaki S, Tagashira K. Macromolecules 2003;36(13):4802–12.
[20] Crist B, Mirabella FM. J Polym Sci Part B Polym Phys 1999;37(21):3131–40.
[21] Clark EJ, Hoffman JD. Macromolecules 1984;17:878–85.
[22] Phillips RA, Wolkowicz MD. Structure and morphology. In: Moore EP, editor. Polypropylene handbook. Munich: Hanser Publishers; 1996. p. 113–76.
[23] Alberola N, Cavaille JY, Perez J. J Polym Sci Part B Polym Phys 1990;28(4):569–86.
[24] Spieckermann F, Wilhelm H, Schafler E, Kerber M, Bernstorff S, Zehetbauer M. 15TH International Conference on The Strength of Materials (ICSMA 15) 16–21. Germany: Dresden; August 2009.
[25] Hoffman JD, Miller RL. Polymer 1997;38(13):3151–212.